POLITECNICO DI TORINO
Repository ISTITUZIONALE

Interfacial Profile and Propagation of Frontal Photopolymerization Waves

Original
Interfacial Profile and Propagation of Frontal Photopolymerization Waves / Vitale, Alessandra; Hennessy, M. G.; Matar, O. K.; Cabral, J. T.. - In: MACROMOLECULES. - ISSN 0024-9297. - ELETTRONICO. - 48:(2015), pp. 198-205. [10.1021/ma5021215]

Availability:
This version is available at: 11583/2588372 since: 2020-01-31T23:03:33Z

Publisher:
ACS American Chemical Society

Published
DOI:10.1021/ma5021215

Terms of use:

This article is made available under terms and conditions as specified in the corresponding bibliographic description in the repository

Publisher copyright

(Article begins on next page)

12 October 2024

This is an open access article published under a Creative Commons Attribution (CC-BY) License, which permits unrestricted use, distribution and reproduction in any medium, provided the author and source are cited.

Macromolecules

Article

pubs.acs.org/Macromolecules

Interfacial Profile and Propagation of Frontal Photopolymerization Waves

Alessandra Vitale, Matthew G. Hennessy, Omar K. Matar, and João T. Cabral*

Department of Chemical Engineering, Imperial College London, London SW7 2AZ, U.K.

Supporting Information

ABSTRACT: We investigate the frontal photopolymerization of a thiol−ene system with a combination of experiments and modeling, focusing on the interfacial conversion profile and its planar wave propagation. We spatially resolve the solid-to-liquid front by FT-IR and AFM mechanical measurements, supplemented by differential scanning calorimetry. A simple coarse-grained model is found to describe remarkably well the frontal kinetics and the sigmoidal interface, capturing the effects of UV light exposure time (or dose) and temperature, as well as the front position and resulting patterned dimensions after development. Analytical solutions for the conversion profile enable the description of all conditions with a single master curve in the moving frame of the front position. Building on this understanding, we demonstrate the design and fabrication of gradient polymer materials, with tunable properties *along* the direction of illumination, which can be coupled with lateral patterning by modulated illumination or grayscale lithography.

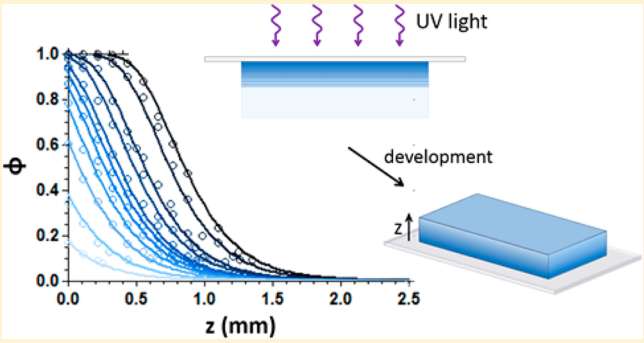

INTRODUCTION

Photoinitiated polymerization of multifunctional monomers provides a facile and rapid method for the synthesis of three-dimensional cross-linked polymer networks.[1,2] Advantages of photopolymerization include that it can be carried out at room temperature, without solvents, and within very short conversion times. UV curing technology has found a large variety of industrial applications, including coatings,[3] adhesives,[4] dental restorative materials,[5] hydrogels,[6] contact lenses,[7] photolithography, and 3D prototyping.[8−10] In particular, thiol−ene (i.e., monomers containing mercapto and vinyl groups) photopolymerization chemistry is relatively well understood.[11−13] Thiol−enes polymerize via a free-radical step growth mechanism and exhibit significant advantages compared to other types of free-radical polymers, such as reduced shrinkage and shrinkage stress, resistance to oxygen inhibition, and the possibility to be photoinitiated even in the absence of a photoinitiator.[14,15]

A promising type of photopolymerization for three-dimensional patterning is the so-called frontal photopolymerization (FPP).[9,16,17] FPP is a process in which polymerization fronts develop and propagate as planar traveling waves into the monomer material, driven by an external light source. FPP occurs in the presence of strong optical attenuation and limited mass and heat transfer, resulting in the formation of a sharp interfacial profile between polymer network and monomer. The solidification front starts from the surface closest to the illuminating source, initially forming a "skin", and then invades the un-cross-linked medium. This frontal aspect of the polymerization process is particularly apparent in the photopolymerization (and cross-linking) of thick (millimeter−centimeter) material sections and permits rapid 3D patterning by modulated or multistep illumination[9] (without resorting to stereo, two-photon, or multistep lithography and alignment). FPP is directional and generally isothermal, being controllably initiated and stopped by collimated light exposure, which is advantageous from a manufacturing perspective.

FPP is a distinct mode of polymerization from thermal (TFP) and isothermal (IFP) frontal polymerizations, which are autocatalytic reaction processes.[18] While these polymerization methods also develop wavelike polymerization fronts, the propagation is (self-)sustained by the thermal energy released from an exothermic polymerization reaction. In TFP, the process is initiated by a localized heat source, and the rate of front propagation is governed by both the rate of thermal diffusion and the nonlinear temperature dependence of the polymerization rate constants. In IFP, also known as "interfacial gel polymerization", the reaction occurs in a viscous fluid or gel matrix that inhibits chain termination (Trommsdorff or "gel" effect), and the polymerization develops into self-sustaining front through the introduction of a polymer "seed". Such frontal polymerization methods have been reviewed by Pojman and co-workers.[18,19]

Received: October 16, 2014
Revised: December 10, 2014
Published: December 22, 2014

Downloaded via POLITECNICO DI TORINO on February 5, 2020 at 15:14:02 (UTC).
See https://pubs.acs.org/sharingguidelines for options on how to legitimately share published articles.

A number of photoinitiation and polymerization models have been reported,[20−26] explicitly addressing the complex chemistry and reaction kinetics of FPP. Some treatments account for photochemical reaction details with various degrees of complexity, including initiator photolysis, chain initiation, propagation, transfer, and termination. The utilization of such models requires the determination of a large number of parameters describing the kinetic coefficients and transport properties and their coupling as these variables change. Given the complexity of these systems, we have previously developed a minimal FPP model[9,16,17] based on physical observables and their evolution in time. In particular, our model describes (i) the position of the solid-to-liquid front z_f, which defines the pattern thickness, and (ii) the light transmission of the material T. The model captures the nonlinear spatiotemporal FPP growth through a system of coupled integrodifferential equations expressing the extent of monomer-to-polymer conversion $\phi(z,t)$ and the optical attenuation $T(z,t)$ as a function of the distance from the illuminating surface z and exposure time t. The order parameter ϕ is normalized such that the boundary conditions are $\phi(z, t = 0) = 0$ and $\phi(z, t = \infty) = 1$. The rate of change of $\phi(z,t)$ is taken to be proportional to the light intensity $I(z,t)$, the fraction of material available for conversion $1 - \phi(z,t)$, and an overall reaction conversion rate K:

$$\frac{\partial \varphi(z, t)}{\partial t} = K[1 - \varphi(z, t)]I(z, t) \tag{1}$$

The transmission T is defined as $T \equiv I(z,t)/I_0$, with $I_0 \equiv I(z = 0)$. The light intensity profile with depth is modeled as a two-component Beer−Lambert law:

$$\frac{\partial I(z, t)}{\partial z} = -\bar{\mu}(z, t)I(z, t) \tag{2}$$

where the effective attenuation coefficient ($\bar{\mu}$) is defined as the weighted average of the attenuation coefficients of the unexposed monomer (μ_0) and polymer material (μ_∞) with composition (ϕ):

$$\bar{\mu}(z, t) \equiv \mu_0[1 - \varphi(z, t)] + \mu_\infty \varphi(z, t) \tag{3}$$

Three possible cases are conceivable within the FPP model, depending on the relative magnitude of the final and initial attenuation coefficients: (i) photoinvariant polymerization, in which the optical attenuation of the polymerized medium is unchanged from the pure monomer ($\mu_0 = \mu_\infty \equiv \bar{\mu}$), (ii) photobleaching, in which the photopolymerized material becomes increasingly transparent to UV radiation during photolysis ($\mu_0 > \mu_\infty$), and (iii) photodarkening, in which the cross-linked material becomes increasingly opaque to UV radiation during polymerization reaction ($\mu_0 < \mu_\infty$). While our FPP model was found to quantitatively describe the (highly nonlinear) solidification kinetics,[9,16] the suitability of the model in predicting the actual spatial conversion profiles has never been evaluated. This is one of the objectives of the paper.

FPP inherently yields a conversion gradient *along* the direction of illumination, which can be further coupled with a *lateral* gradient, imposed by a photomask. Gradient polymer materials, exhibiting property gradients (optical, rheomechanical, etc.) in one or more dimensions, have generated great interest in recent years[27−29] owing to the potential of rapidly manufacturing systems with customized, modulated properties for different applications, including fabrication of organic optical limiters,[30] direct assembling of soft materials,[31] and directed cell growth within tissue-engineered scaffolds.[32]

In this work, we explicitly investigate the interfacial profiles generated by FPP, the factors governing the profile shape and propagation, and the conditions relevant for pattern development (by selective dissolution) and thus manufacturing. In order to fabricate gradient materials, we seek to tune precisely the conversion profiles along the sample depth controlling the UV curing conditions (including time, intensity, and temperature of irradiation). While photopolymerization profiles have been previously modeled[33−35] and investigated experimentally,[36,37] we are not aware of a detailed, combined experimental and modeling study of spatiotemporal polymerization kinetics. We find that the FPP model can describe the evolution of the front profile of a thiol−ene system with remarkable accuracy, despite its simplicity (effectively combining all steps into a single kinetic constant K and neglecting mass and thermal diffusion). Building on this understanding, we demonstrate the design of a polymer network with a gradient of mechanical modulus.

■ EXPERIMENTAL SECTION

Materials and Methods. A multifunctional thiol−ene based optical adhesive (NOA81, Norland Products) was used as the photopolymerizable material for this study. It is an optically clear UV-curable prepolymer with relatively low viscosity (0.3 Pa s) and good adhesion to glass and metal surfaces. The material exhibits high sensitivity to long wavelength UV radiation (sensitivity peak around 365 nm). Once cured, the resulting solid network has a rather high modulus and becomes insoluble to an array of solvents (including toluene, methanol, hexane, and methyl ethyl ketone, but excluding chlorinated solvents). However, the uncured prepolymer remains soluble in ethanol and acetone, which we used as developers. The UV source used for photopolymerization is a monochromatic 365 nm Spectroline SB-100P flood lamp, equipped with a 100 W mercury lamp (Spectronics). Light intensity was measured with a UVItec RS-365 digital radiometer. Polydimethylsiloxane (PDMS) Sylgard 184 elastomer kit was purchased from Dow Corning. All other chemicals were obtained from VWR Chemicals.

The prepolymer was placed between a glass slide (top surface) and thermally cured PDMS (bottom surface) with a spacer between them (3 mm thick PDMS membranes were cut in frames and used as gasket materials). Photocuring was carried out for different exposure times t (5−5000 s) and sample-to-lamp distances to adjust the incident intensity (I_0 = 0.3−1 mW cm^{-2}). A wide UV dose ($d \equiv I_0 \times t$) window covering 0−5 J cm^{-2} was investigated. For the photopolymerization experiments at high temperature, we used a hot plate to heat up the system and a RayTemp8 infrared thermometer to control the prepolymer temperature. Development of the patterned polymer networks was performed with acetone and ethanol to remove un-cross-linked material.

Characterization. The thickness of the cross-linked samples was measured with a reflection optical microscope (Olympus BX41M) and, for large thicknesses, with a digital caliper. At least five measurements were recorded to calculate mean and maximum error.

The photopolymerization conversion (χ) was monitored by Fourier transform infrared (FT-IR) spectroscopy, using a Bruker Tensor 27 spectrometer equipped with a Hyperion microscope. The cross-linked samples were cryofractured in thin (about 200 μm) slices along their depth (z) with liquid nitrogen. For each sample different spectra were acquired along z. The decrease of the area of the absorption band of reactive functionality (thiol groups centered at 2572 cm^{-1}) was observed. A reference band at 1735 cm^{-1}, assigned to carbonyl groups, was used to calculate conversions in $\Delta z \approx 50$ μm steps, corresponding to the FT-IR field of view. The conversion of the material was determined as follows:

$$\chi(z, t) = \left.\frac{A_0^{2572}/A_0^{1735} - A_t^{2572}/A_t^{1735}}{A_0^{2572}/A_0^{1735}}\right|_z \quad (4)$$

where A_0 is the initial absorbance (before UV irradiation) and A_t is the absorbance at time t.

The conversion on the sample surfaces (both the one in contact with the glass substrate and the one in contact with the liquid prepolymer during photopolymerization) was measured by means of a FT-IR spectrometer (PerkinElmer Spectrum 100), equipped with a Specac attenuated total reflection (ATR) unit.

Differential scanning calorimetry (DSC) curves were recorded using a TA Instruments DSC Q2000 in nitrogen in the temperature range −100 to 150 °C using a cool/heat method at a scanning rate of 10 °C min^{-1}. DSC analyses were performed on thin (100 μm) UV cured films, which could be considered uniformly cross-linked. The glass transition temperature (T_g) was determined using the midpoint method on the heating cycle thermogram.

Elastic moduli of the cured materials were measured by atomic force microscopy (AFM) with a Bruker Innova instrument. The optical microscope enabled us to position the AFM tip on the area of interest of the sample. Force curves were acquired along the sample depth (z). FESPA and TESPA silicon probes (Bruker) with rectangular shape, tip side angle of 22.5°, and spring constant of 2.8 and 42 N m^{-1}, respectively, were used. Cantilevers were calibrated by measuring the thermally induced motion of the unloaded cantilever.[38] The Young's modulus E was calculated following the Sneddon model[39,40] for a cone pushing into a flat surface.

■ RESULTS AND DISCUSSION

Our FPP experimental setup is depicted in Figure 1. The planar polymerization wave emanates from the top, illuminated, transparent surface which anchors the growing solid network. The polymerization front propagation generates a nonlinear profile of the monomer-to-polymer conversion ϕ within the material. After UV exposure and development to remove the uncured prepolymer, a gradient cross-linked polymer is obtained. FPP reaction confined between two surfaces (e.g., glass), and modulated through a photomask, readily yields microfluidic devices by ultrarapid prototyping.[9] In this work, we use a commercial thiol−ene system as the photopolymerizable resin, characterized by optical clarity and negligible shrinkage upon curing (Supporting Information Figure S1), whose propagation kinetics has been previously reported.[9,16]

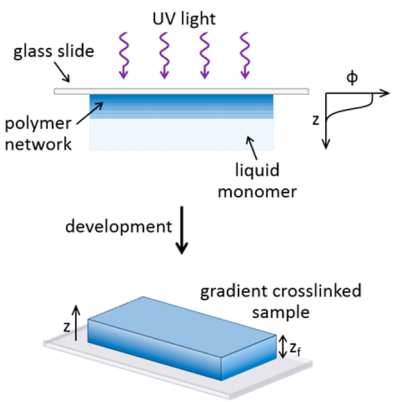

Figure 1. Schematic of the FPP experimental setup showing the photopolymerization front propagation from the UV illuminated surface and the profile of the extent of monomer-to-polymer conversion ϕ within the network. After UV exposure and development (to remove the uncured prepolymer), samples with thickness z_f and displaying a cross-linking gradient in z (along their depth) are obtained.

We first confirm the frontal nature of photopolymerization process by measuring the solid thickness of different samples exposed to UV light for increasing time intervals. We confirm that exposure time t and UV dose d can effectively be used interchangeably, as the dose (the product of light intensity and exposure time, $d \equiv I_0 \times t$) controls the front kinetics. The thickness of the resulting cured films (z_f), corresponding to the front position after development, grows logarithmically with d (Figure 2a), consistent with previous results.[9,16] Controlling the dose transferred to the prepolymer yields film thicknesses ranging from a few microns to millimeters. Figure 2a also shows that the formation of a solidification front does not occur instantaneously with light exposure, and a threshold UV dose is required before a solid front (a "skin") starts propagating from the illuminated surface. Below 9.6 ± 1.0 mJ cm^{-2} (corresponding to $t \approx 32$ s at 0.3 mW cm^{-2}) the material is washed away upon development, defining its critical dose d_c for the onset of frontal propagation. The dose d_c corresponds to a critical conversion fraction ϕ_c: below ϕ_c the material is soluble upon development, while above ϕ_c it is insoluble. The position of the solid/liquid interface front z_f (corresponding to the sample thickness after exposure and development) is defined implicitly when ϕ reaches ϕ_c, i.e., $z_f \equiv z(\phi = \phi_c)$.

According to the FPP model,[16] the inverse of the slope ($1/\mu$) of the curve in Figure 2a corresponds to the optical attenuation coefficient μ (μ = 3.7 ± 0.2 mm^{-1}). From the experimental data, it is clear that μ remains constant in the dose range considered, effectively corresponding to photoinvariant polymerization conditions ($\mu_0 = \mu_\infty \equiv \bar{\mu}$). In the photoinvariant case, the system of eqs 1 and 2 of the FPP model can be solved analytically, and the conversion fraction in this case becomes[16]

$$\varphi(z, t) = 1 - \exp[-KI_0 \exp(-\mu z)t] \quad (5)$$

and the front position z_f, corresponding to the solidified thickness, is given by

$$z_f = \frac{\ln\left[\frac{KI_0 t}{\ln\left(\frac{1}{1-\varphi_c}\right)}\right]}{\mu} \quad (6)$$

Substituting eq 6 into eq 5 returns the critical conversion fraction ϕ_c imposed above:

$$\varphi_c = 1 - \exp[-KI_0 \exp(-\mu z_f)t] \quad (7)$$

Experimental data of Figure 2a could be described using ϕ_c = 0.052 ± 0.002. Parameters ϕ_c and KI_0 are coupled and previously could only be resolved by self-consistency of numerous measurements.[9,16] Given our ability to spatially resolve the actual interfacial profile $\phi(z,t)$, we first determine KI_0 by fitting eq 5 and then unequivocally determine ϕ_c by either locating the minimum conversion at the solid/liquid interface or substituting the measured z_f and KI_0 into eq 7. Further details of this procedure and parameter sensitivity are included in Supporting Information (Figure S2a,b).

Interfacial Profile. In order to precisely characterize the gradient obtained throughout the photocured material, we measured the monomer-to-polymer conversion along the sample thickness, indicated as z (see Figure 1). The conversion χ, measured by FT-IR spectroscopy, was calculated as the decrease of the thiol absorption peak (centered at 2572 cm^{-1})

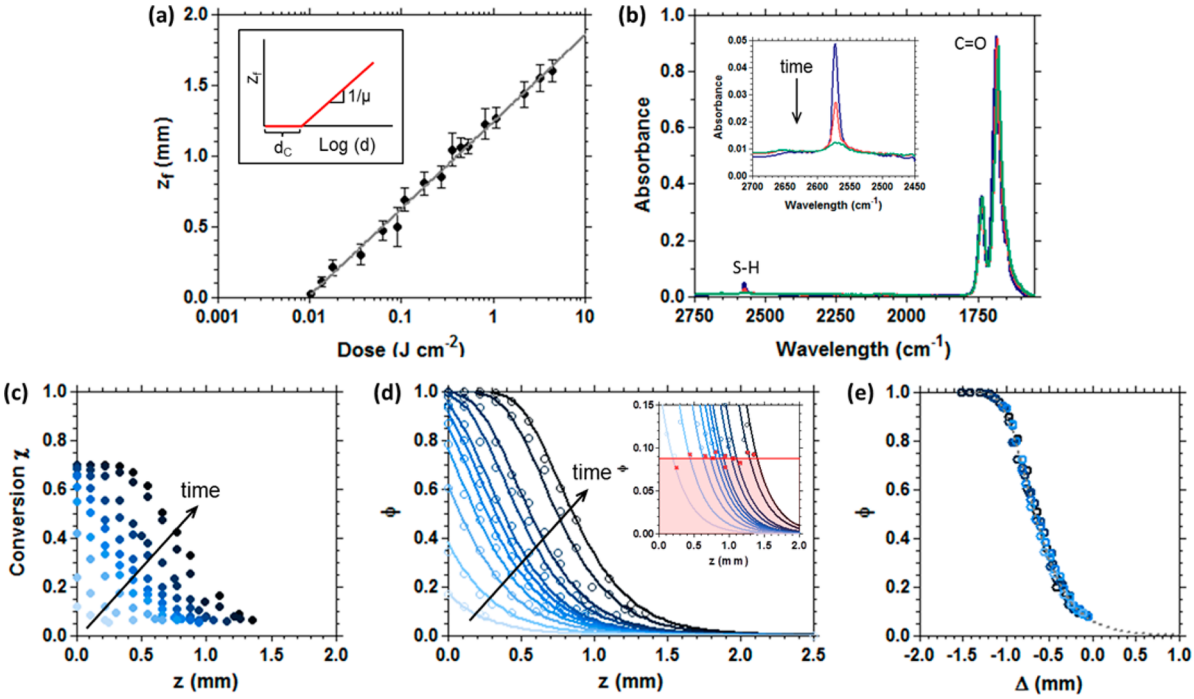

Figure 2. FPP frontal kinetics for a thiol−ene system measured at room temperature (T = 23 °C). (a) Sample height $z_f(t)$ dependence on UV dose d, exhibiting logarithmic growth with proportionality constant $1/\mu$. This trend is representative of the photoinvariant polymerization, in which transmission remains constant upon UV exposure. The UV dose window 0.01−4.5 J cm^{-2} was obtained using a light intensity of 0.3 or 0.9 mW cm^{-2} and varying the exposure time (from 5 to 5000 s). (b) FT-IR spectra of the thiol−ene material used to measure the polymerization conversion χ. The inset details the decrease of the thiol (S−H) absorption peak (centered at 2572 cm^{-1}) with time. The constant carbonyl (C═O) band was used as reference. The three spectra correspond to samples irradiated for different times: d = 0 J cm^{-2} (blue line), d = 0.18 J cm^{-2} (red line), and d = 0.81 J cm^{-2} (green line). (c) Conversion χ profiles along the sample depth z for increasing UV irradiation time t (corresponding to a dose range of 0.036−3.24 J cm^{-2}). (d) Extent of conversion $\phi(z,t) \equiv \chi(z,t)/\chi_{max}$ dependence on z and t. Dots are experimental data, while solid lines are model fits. The inset details the intersection of the solid conversion threshold ϕ_c with $\phi(z,t)$, defining the front position $z_f(t)$. Photopolymerization was performed with a dose range of 0.036−3.24 J cm^{-2}. (e) Master curve representing the extent of conversion $\phi(z,t)$ as a function of the coordinate of the moving front $\Delta \equiv z - z_f$.

with irradiation dose (or time). Figure 2b reports the spectrum evolution of the thiol−ene material: increasing the UV dose, the area of the thiol peak diminishes (inset of Figure 2b) as S−H groups take part in the curing reaction, while the area of the carbonyl peak remains nearly constant. The experimentally measured conversion χ profiles along z for samples UV irradiated at room temperature with an increasing dose value (ranging from 0.036 to 3.24 J cm^{-2}) are shown in Figure 2c. As expected, a conversion gradient was obtained for all samples, whose extent depends on UV curing conditions. The conversion at the solid/liquid interface (χ_c) is 0.062, as estimated by FT-IR ATR measurements from the top surface of the solidified sample. This value is much lower than the gel point conversion expected for multifunctional thiol−ene systems by the Flory−Stockmayer theory.[41,42] This is unsurprising since our photocurable system comprises oligomeric species ("prepolymers"), instead of a mixture of reactive multifunctional monomers.

We defined the extent of polymerization $\phi(z,t)$ as the normalized conversion χ measured experimentally, i.e., $\phi(z,t) \equiv \chi(z,t)/\chi_{max}$, where χ_{max} has been determined to be 0.7 for this data series. Calculated ϕ values as a function of z and UV irradiation time t are reported in Figure 2d (points). We then fitted the calculated ϕ data with eq 5 of the FPP model, and the resulting profiles are shown as solid lines in the figure. These were obtained using the experimentally measured attenuation coefficient μ and the fitting parameter KI_0 = 0.0016 s^{-1}. The agreement between model results and experimental data is remarkable, in particular given the simplicity of the theoretical assumptions. Normalized conversion $\phi(z,t)$ exhibits a simple sigmoidal form and translates logarithmically in time with a time-invariant shape, although the full front does not enter into the positive z-axis until a sufficient dose has been reached. From data reported in Figure 2d we find an upper estimate for the critical ϕ_c value to be ≤0.088, which corresponds to the average of the minimum measured ϕ values (see inset). This estimate agrees well with the value of ϕ_c reported before from fitting front position kinetics (ϕ_c = 0.052 ± 0.002).

Conversion profiles can be rescaled equivalently in terms of the coordinate Δ moving with the polymerization front: $\Delta \equiv z - z_f$. Figure 2e shows the master curve obtained representing the experimental ϕ data as a function of Δ. The normalized conversion $\phi(z,t)$ propagates as a moving sigmoidal-shaped front whose position is defined by z_f, corresponding to the critical conversion point ϕ_c of the front that advances in space. Similar results can be obtained defining the front position with different criteria (Supporting Information, Figure S3). For this system, the interfacial width is of the order of 1 mm.

Effect of Temperature on Front Profile. At increasing temperatures, the FPP reaction generally proceeds faster, yielding thicker solid samples for a fixed UV dose. In agreement with our previous work,[16] $z_f(t)$ still grows logarithmically with the dose, but more rapidly, as illustrated in Figure 3a for T = 23 °C and T = 100 °C. The slope of the two logarithmic profiles

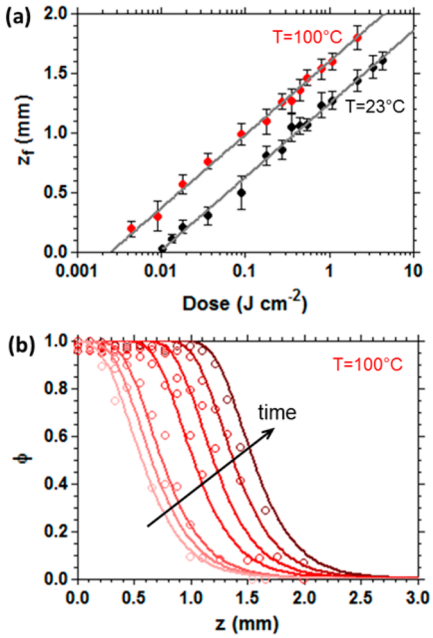

Figure 3. FPP frontal kinetics for polymerizations performed at high temperature. (a) Comparative sample height $z_f(t)$ dependence on UV dose for T = 23 °C and T = 100 °C, exhibiting logarithmic kinetics with nearly constant slope $(1/\mu)$. UV irradiation was performed with light intensity I_0 = 0.3 mW cm^{-2} (for low doses) or 0.9 mW cm^{-2} (for high doses) and varying the exposure time (150−2400 s). (b) Extent of conversion ϕ profiles along the sample depth z for increasing UV irradiation time t (corresponding to a dose range of 0.045−2.16 J cm^{-2}). Points are experimental data, while solid lines are model fits to eq 5. Photopolymerization was conducted at T = 100 °C.

$(1/\mu)$ is nearly constant, indicating that the attenuation coefficient μ does not change with temperature, as expected for a material property. By contrast, the critical UV dose d_c decreases with increasing temperature, and we find $d_c(T = 23\ °C) = 9.6 \pm 1.0$ mJ cm^{-2} and $d_c(T = 100\ °C) = 2.1 \pm 0.6$ mJ cm^{-2} for the two profiles in Figure 3a.

In order to evaluate the effect of temperature on the interfacial profiles and master curve, we measured by FT-IR the conversion along the thickness (z-direction) for samples polymerized at T = 100 °C. Also in this case, the ϕ experimental values are found to be in good agreement with the FPP model (Figure 3b), even though the level of agreement is poorer than at lower temperatures. This may be due to finite heat and mass transfer or to the onset of an interfacial instability at sufficiently high temperatures that disrupts strict planar propagation. The data of Figure 3b were described by KI_0 = 0.0438 s^{-1} as a fitting parameter, higher than the value found at 23 °C, at constant I_0. We find that the solidification threshold measured at the polymer/liquid interface does not depend on temperature, i.e., $\chi_c(T = 100\ °C) = 0.069$, as could be expected for a network property, depending only on the chemical structure of the prepolymer.

Figure 4a depicts the front position z_f obtained at increasing temperatures for a fixed dose (d = 1.08 J cm^{-2}). Above 100 °C the reaction equilibrium shifts, altering the monotonic trend. In the following, we have thus considered only the temperature range 23−100 °C. In Figure 4b are represented the conversion χ values measured by FT-IR for the fixed dose d = 1.08 J cm^{-2} as a function of temperature, corresponding to the specimens in Figure 4a. We find that the maximum conversion, obtained on the surface closest to the illuminating source (z = 0), increases with temperature. It appears that larger mobility afforded at high temperature permits achieving marginally larger conversion of polymer network. In order to obtain ϕ values, each

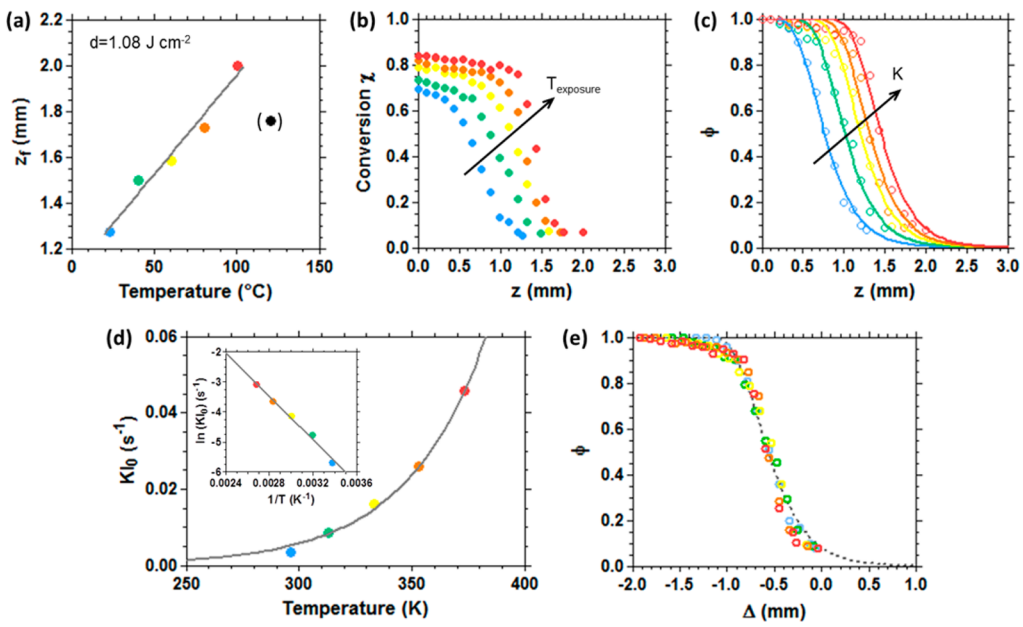

Figure 4. Influence of temperature on FPP kinetics at fixed UV light dose (d = 1.08 J cm^{-2}) within temperature range 23−100 °C. (a) Front position (determined as the developed sample thickness) z_f as a function of temperature of polymerization T. (b) Dependence of conversion χ profiles (measured by FT-IR) on curing temperature along sample depth z. (c) Normalized conversion ϕ dependence on z and T. Points are experimental data, while solid lines are model fits. (d) Kinetics constant KI_0 as a function of photopolymerization temperature, showing an Arrhenius behavior (depicted in the inset). (e) Master curve representing ϕ, at all studied temperatures, rescaled in the coordinate of the moving front Δ ($\Delta \equiv z - z_f$) by the parameters in (d).

series was thus normalized separately by the respective χ_{max} for each temperature. The normalized front profiles, depicted in Figure 4c, were then individually fitted to a different parameter KI_0. At a fixed dose, we find that KI_0 increases exponentially with temperature, as shown in Figure 4d. KI_0 can be in fact considered an overall polymerization kinetics constant, and the data are well fitted to an Arrhenius form (inset in Figure 4d). Close inspection of Figure 4c indicates that upon increasing the curing temperature, the experimental data deviate gradually from the fitting model, which we have associated with finite heat and mass transfer processes. Rescaling all data in the moving coordinate frame Δ yields a well-defined master frontal profile in Figure 4e, characterizing the frontal shape and propagation of this thiol−ene system. Alternative front position criteria, including the inflection point, yield similar results (detailed in Supporting Information, Figure S4).

The isothermal nature of this FPP system, at four representative temperatures (20−80 °C), was ascertained by monitoring the local temperature variation during wave propagation, which is found to be minimal, ΔT = 0−2 °C (Supporting Information, Figure S5). We can thus exclude nontrivial autoacceleration effects (characteristic of the Trommsdorff−Norrish effect) in our FPP kinetics modeling.

After demonstrating that gradient cross-linked polymers can be easily obtained by FPP, we have studied the thermal and mechanical properties of the resulting materials. In particular, we also seek to elucidate whether the solidification front corresponds to a gelation or glass-formation condition. We have thus measured the glass transition temperature of sufficiently thin polymer films (approximately 100 μm) to be considered homogeneously cross-linked. We computed separately their degree of conversion by FT-IR and plotted the combined results in Figure 5a. The experimental data are well described by a geometric average (analogous to a Flory−Fox relationship), calculated between the T_g value of the liquid prepolymer (−60.7 °C) and the T_g value of a cross-linked polymer network with χ = 0.824 (28.7 °C). We conclude that the networks only become glassy at very large conversions (χ > 0.79). At very low conversions, below the critical threshold χ_c (χ < 0.062), the material is a liquid. For most of the conversion range accessible 0.062 < χ < 0.79, we thus obtain a polymer network below its glass transition. During the course of light exposure, the liquid−solid transition is found to occur via gelation at an early stage, followed by a glass transition at much longer exposure times, at sufficiently low temperatures (≤40 °C).

Simultaneously plotting the conversion profiles obtained for samples cured at different temperatures and the corresponding T_g values (Figure 5b), it is clear that we can controllably design gradient material properties with well-defined depth profiles, ranging from a stratified glass-to-elastomer (higher UV curing temperature) to a gradient elastomer profile (lower UV curing temperature).

Similarly, the mechanical properties display a gradient profile along the sample thickness, accompanying conversion. We measured the local Young's modulus E along the cross section of the film by AFM force−distance measurements, depicted in Figure 6a. The mechanical properties of the two faces of one sample can be designed to be very different: gradually ranging from a soft surface, across the material depth, to a rigid opposite surface. Selecting the UV curing temperature, it is possible to control the mechanical properties of the final material and its profile. For instance, increasing the temperature

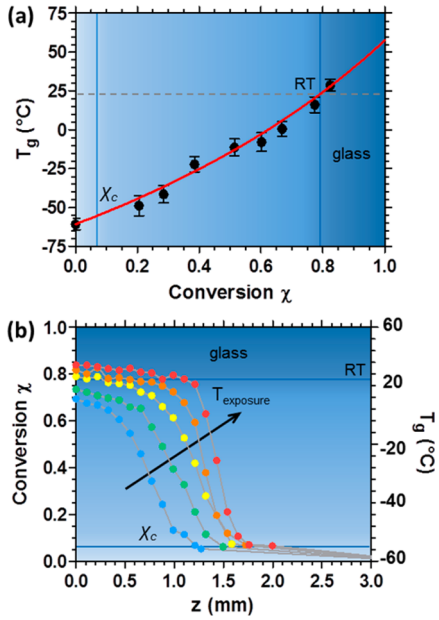

Figure 5. (a) Dependence of glass transition temperature of the material on conversion. The data follow a geometric average trend (solid line). (b) Conversion χ profiles along the sample depth z for increasing UV exposure temperature within 23−100 °C, correlated with the T_g of the polymer. At high conversion (T_g > RT) the material is a rigid cross-linked glassy polymer (dark blue), then a flexible elastomer at lower χ values (blue), and finally a liquid when $\chi < \chi_c$ (light blue).

from 23 to 100 °C, the modulus of the surface closest to the illuminating source (z = 0) increases 7-fold, while the gradient becomes similarly more pronounced. In Figure 6b the Young's modulus is reported as a function of conversion χ for different UV curing temperatures. In all cases, E slightly increases with χ until around χ = 0.75 and then grows much faster, as the network's T_g exceeds room temperature when χ > 0.79 and the material vitrifies. The surface tackiness and adhesion qualitatively follow the reverse trend suggesting possible applications in supported gradient adhesives.

The gradient *along* the direction of illumination, given naturally by FPP reaction and controlled by parameters KI_0 and μ, can be further coupled with a *lateral* gradient imposed by a grayscale photomask. We demonstrate this approach by FPP patterning through a circular gradient mask with optical density increasing radially (further examples of gradient and step patterns are provided in Supporting Information, Figure S6). The resulting pattern and measured conversion profiles in x, y, and z are shown in Figure 6c. Curved, lens-shaped features exhibiting well-defined conversion gradients in all directions are readily fabricated.

■ CONCLUSIONS

We have directly resolved the interfacial profiles and propagation kinetics during frontal photopolymerization (FPP) using a thiol−ene model system. The experimentally measured conversion profiles in the resulting gradient polymer networks and frontal kinetics were found to be quantitatively well-described by our coarse-grained FPP model. Depth conversion profiles are governed by optical attenuation and reaction kinetics, modeled by parameters μ and KI_0, and front position can be finely controlled by changing photopolymerization conditions (including time and temperature of irradiation).

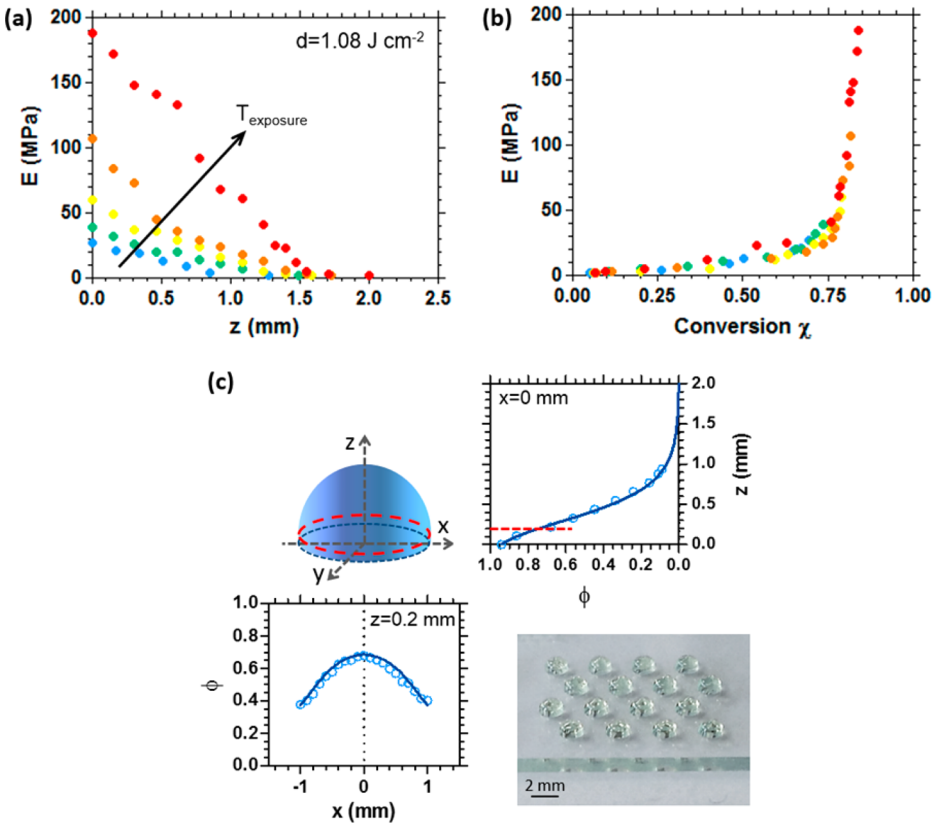

Figure 6. Mechanical properties of the gradient cross-linked photopolymer and three-dimensional gradients. (a) Young's modulus E profile along the sample depth z for materials UV cured at different temperatures (temperature range 23−100 °C) and with fixed UV light dose (d = 1.08 J cm^{-2}). (b) E as a function of the polymer conversion. (c) Exemplar of an FPP gradient pattern obtained by grayscale lithography yielding a lens-shaped pattern with tunable conversion gradients in all directions: along z (sample height) and along x and y (lateral dimensions). The data points in the graphs are normalized conversion ϕ measured by FT-IR along z (defined by x, y = 0, 0 mm) and along an x line (defined by y, z = 0, 0.2 mm). Solid lines are model predictions based on our FPP model and parameters determined above.

An understanding of FPP enables the design of thermal and rheomechanical properties of the gradient polymer networks, by tuning conversion profile across a critical threshold and glass formation conditions. We finally demonstrate the FPP fabrication of gradient cross-linked polymers *along* the light propagation direction, which can further be coupled to lateral spatial gradients through grayscale photomask pattern transfer.

■ ASSOCIATED CONTENT

Ⓢ Supporting Information

Evaluation of ϕ_c and KI_0 parameters and rescaling in the coordinate of the moving front, photopolymer shrinkage study, temperature evolution during FPP and further examples of gradient and step patterns. This material is available free of charge via the Internet at http://pubs.acs.org.

■ AUTHOR INFORMATION

Corresponding Author

*E-mail: j.cabral@imperial.ac.uk (J.T.C.).

Notes

The authors declare no competing financial interest.

■ ACKNOWLEDGMENTS

We thank EPSRC for a "Manufacturing with Light" grant EP/L022176/1 and Jack. F. Douglas (NIST) for stimulating discussions. We acknowledge K. Kaja (Bruker) for helpful assistance in AFM force spectroscopy.

■ REFERENCES

(1) Fouassier, J. P.; Allonas, X. *Basics and Applications of Photopolymerization Reactions*; Research Signpost: Trivandrum, India, 2010.
(2) Decker, C. *Polym. Int.* **2002**, *51* (11), 1141−1150.
(3) Davidson, R. S. *Exploring the Science, Technology and Applications of UV and EB Curing*; Sita Technology Limited: Pretoria, South Africa, 1999.
(4) Yacobi, B. G.; Martin, S.; Davis, K.; Hudson, A.; Hubert, M. *J. Appl. Phys.* **2002**, *91* (10), 6227−6262.
(5) Stansbury, J. W.; Bowman, C. N.; Newman, S. M. *Phys. Today* **2008**, *61*, 82−83.
(6) Wichterle, O.; Lim, D. *Nature* **1960**, *185* (4706), 117−118.
(7) McMahon, T. T.; Zadnik, K. *Cornea* **2000**, *19* (5), 730−740.
(8) Hutchison, J. B.; Haraldsson, K. T.; Good, B. T.; Sebra, R. P.; Luo, N.; Anseth, K. S.; Bowman, C. N. *Lab Chip* **2004**, *4*, 658−662.
(9) Cabral, J. T.; Hudson, S. D.; Harrison, C.; Douglas, J. F. *Langmuir* **2004**, *20* (23), 10020−10029.
(10) Vitale, A.; Quaglio, M.; Marasso, S. L.; Chiodoni, A.; Cocuzza, M.; Bongiovanni, R. *Langmuir* **2013**, *29* (50), 15711−15718.
(11) Cramer, N. B.; Davies, T.; O'Brien, A. K.; Bowman, C. N. *Macromolecules* **2003**, *36* (12), 4631−4636.
(12) Hoyle, C. E.; Lee, T. Y.; Roper, T. *J. Polym. Sci., Part A: Polym. Chem.* **2004**, *42* (21), 5301−5338.
(13) Reddy, S. K.; Okay, O.; Bowman, C. N. *Macromolecules* **2006**, *39* (25), 8832−8843.
(14) Cramer, N. B.; Scott, J. P.; Bowman, C. N. *Macromolecules* **2002**, *35* (14), 5361−5365.
(15) Bowman, C. N.; Kloxin, C. J. *AlChE J.* **2008**, *54* (11), 2775−2795.

(16) Cabral, J. T.; Douglas, J. F. *Polymer* **2005**, *46* (12), 4230−4241.
(17) Warren, J. A.; Cabral, J. T.; Douglas, J. F. *Phys. Rev. E* **2005**, *72* (2), 021801.
(18) Pojman, J. A. 4.38 - Frontal Polymerization. In *Polymer Science: A Comprehensive Reference*; Möller, K. M., Ed.; Elsevier: Amsterdam, 2012; pp 957−980.
(19) Khan, A.; Pojman, J. The Use of Frontal Polymerization in Polymer Synthesis. In *Trends in Polymer Science*; Elsevier Trends Journals: Cambridge, 1996; Vol. *4*, pp 253−257.
(20) Rytov, B. L.; Ivanov, V. B.; Ivanov, V. V.; Anisimov, V. M. *Polymer* **1996**, *37* (25), 5695−5698.
(21) Terrones, G.; Pearlstein, A. J. *Macromolecules* **2001**, *34* (10), 3195−3204.
(22) Terrones, G.; Pearlstein, A. J. *Macromolecules* **2001**, *34* (26), 8894−8906.
(23) Terrones, G.; Pearlstein, A. J. *Macromolecules* **2003**, *36* (17), 6346−6358.
(24) Terrones, G.; Pearlstein, A. J. *Macromolecules* **2004**, *37* (4), 1565−1575.
(25) Ivanov, V. V.; Decker, C. *Polym. Int.* **2001**, *50* (1), 113−118.
(26) Miller, G. A.; Gou, L.; Narayanan, V.; Scranton, A. B. *J. Polym. Sci., Part A: Polym. Chem.* **2002**, *40* (6), 793−808.
(27) Désilles, N.; Lecamp, L.; Lebaudy, P.; Bunel, C. *Polymer* **2003**, *44* (20), 6159−6167.
(28) Hansen, A.; Zhang, R.; Bradley, M. *Macromol. Rapid Commun.* **2012**, *33* (13), 1114−1118.
(29) Chen, C.; Liu, J.; Sun, F.; Stansbury, J. W. *RSC Adv.* **2014**, *4* (55), 28928−28936.
(30) Masere, J.; Lewis, L. L.; Pojman, J. A. *J. Appl. Polym. Sci.* **2001**, *80* (4), 686−691.
(31) Nakanishi, H.; Namikawa, N.; Norisuye, T.; Tran-Cong-Miyata, Q. *Soft Matter* **2006**, *2* (2), 149−156.
(32) Turturro, M. V.; Papavasiliou, G. *J. Biomater. Sci., Polym. Ed* **2012**, *23* (7), 917−939.
(33) Lecamp, L.; Lebaudy, P.; Youssef, B.; Bunel, C. *Macromol. Symp.* **1999**, *148* (1), 77−86.
(34) Hayki, N.; Lecamp, L.; Désilles, N.; Lebaudy, P. *Macromolecules* **2009**, *43* (1), 177−184.
(35) Bayou, S.; Mouzali, M.; Aloui, F.; Lecamp, L.; Lebaudy, P. *Polym. J.* **2013**, *45* (8), 863−870.
(36) Désilles, N.; Lecamp, L.; Lebaudy, P.; Bunel, C. *Polymer* **2004**, *45* (5), 1439−1446.
(37) Tao, Y.; Yang, J.; Zeng, Z.; Cui, Y.; Chen, Y. *Polym. Int.* **2006**, *55* (4), 418−425.
(38) Butt, H. J.; Jaschke, M. *Nanotechnology* **1995**, *6* (1), 1.
(39) Sneddon, I. N. *Int. J. Eng. Sci.* **1965**, *3* (1), 47−57.
(40) Oliver, W. C.; Pharr, G. M. *J. Mater. Res.* **2004**, *19* (01), 3−20.
(41) Flory, P. J. *J. Am. Chem. Soc.* **1941**, *63* (11), 3083−3090.
(42) Stockmayer, W. H. *J. Chem. Phys.* **1943**, *11* (2), 45−55.